Cluster Structures of Supercritical CH_4 Confined in Carbon Nanospaces with in Situ High-Pressure Small-Angle X-ray Scattering and Grand Canonical Monte Carlo Simulation

T. Ohba,[†] T. Omori,[†] H. Kanoh,[†,‡] and K. Kaneko*[,†,‡]

Department of Chemistry, Faculty of Science, Chiba University, 1-33 Yayoi, Inage, Chiba 263-8522, Japan, and Center for Frontier Electronics and Photonics, Chiba University, 1-33 Yayoi, Inage, Chiba 263-8522, Japan

Received: August 9, 2003; In Final Form: October 29, 2003

The cluster structures of supercritical CH_4 confined in slit-shaped carbon micropores was investigated using in situ small-angle X-ray scattering (SAXS) and the cluster analysis for grand canonical Monte Carlo (GCMC) simulation. The pore size distribution of micropores was determined from the fitting of the GCMC-simulated adsorption isotherm to the experimental one for high-pressure CH_4; the pore size distributions of two kinds of activated carbon fibers (ACFs) were very narrow, and their average widths are 0.6 and 1.1 nm. The density fluctuation changes with fractional filling from in situ SAXS and GCMC simulation evidenced explicitly the formation of clusters of high concentration in the micropores. CH_4 molecules in smaller pores of 0.6 nm form highly concentrated clusters even in low fractional filling. Fewer clusters are formed in the case of wider pores of 1.1 nm.

1. Introduction

Although natural gas (NG) has been requested to apply to vehicular fuel from an environmental point of view, the volumetric energy density at an ambient temperature must be improved using compressed natural gas (CNG) at 25 MPa or adsorbed natural gas (ANG) with microporous materials. As the CNG needs the high-pressure facilities and tanks of a sufficient safety, ANG has merits for large-scale applications.[1−4] However, we do not have microporous adsorbents storing methane enough to be applied. Therefore, a fundamental study on adsorption mechanism of supercritical methane can encourage the development of optimum microporous systems.[5−7] Activated carbon fiber (ACF) has considerably uniform slit-shaped micropores of great capacity. Furthermore, ACFs of different pore width in the range of 0.7−1.4 nm are available for fundamental studies. These authors have elucidated the adsorbed structure of vapor molecules in micropores of ACF using in situ X-ray diffraction, showing the solidlike structures for water,[8,9] SO_2,[10] and alcohol.[11,12] Recently, Iiyama et al. showed the effectiveness of in situ small-angle X-ray scattering (SAXS) for elucidation of the adsorption mechanism for water vapors in micropores of ACF.[9] The preceding studies showed that ACF is a good adsorbent for methane.[13−15] Accordingly, we extended the in situ SAXS technique to study the adsorbed states of supercritical methane in micropores of ACF under the high pressure. The information from the in situ SAXS can be associated with the intermolecular structures of the snapshots from grand canonical Monte Carlo (GCMC) simulation.[16−18] This paper describes cluster structures of supercritical methane adsorbed in micropores of activated carbon fibers (ACFs) with in situ high-pressure SAXS and GCMC simulation.

* To whom correspondence should be addressed. Fax: 81-43-290-2788. E-mail: kaneko@pchem2.s.chiba-u.ac.jp.
† Department of Chemistry.
‡ Center for Frontier Electronics and Photonics.

2. Experiment, Analysis, and Simulation

Pitch-based ACFs (P5 and P20) of different pore widths were used for high-pressure CH_4 adsorption and in situ SAXS measurements. The high-pressure adsorption isotherms of methane were measured by use of a Cahn balance gravimetrically at 303 K. The micropore structures of ACFs were determined by N_2 adsorption measurement at 77 K and adsorption of supercritical CH_4 itself at 303 K.

The SAXS experiments were performed on the apparatus having a two axial system with three slits. The specially designed sample cell for the high-pressure adsorption up to 5 MPa was used. The radiation was Cu Kα of which the wavelength, λ, is 0.1542 nm. Scattered X-ray were detected by a position-sensitive proportional counter in the scattering angular range of $\theta = 0.2-5°$. Thus, the measured range of the scattering parameter, $s = 4\pi \sin\theta/\lambda$, was from 0.28 to 7.1 nm^{-1}. ACFs were pretreated at 383 K and 1 mPa for 2 h prior to these measurements.

Density fluctuation and correlation length were determined from Ornstein−Zernike (OZ) analysis of the SAXS profile near $s = 0$ described by eq 1.[9,19,20]

$$I(s) = \frac{I(0)}{1 + \xi^2 s^2} \tag{1}$$

Here, ξ and $I(0)$ are the OZ correlation length and the scattering intensity at $s = 0$, respectively. OZ plots are given by transformation of eq 1.

$$\frac{1}{I(s)} = \frac{1}{I(0)} + \frac{\xi^2}{I(0)} s^2 \tag{2}$$

The value of ξ is an approximated scale of the heterogeneous structures of electron density; it can be used for estimation of the cluster size, if adsorbed molecules form their clusters in the pores. The relationship between the density fluctuation

10.1021/jp0363646 CCC: $27.50
Published on Web 12/05/2003

$\langle(\Delta N)^2\rangle/N$ and $I(0)$ is given by eq 3.

$$\frac{I(0)}{N} = Z^2\frac{\langle(\Delta N)^2\rangle}{N} \tag{3}$$

Here, N and Z are the number of molecules and the number of electrons in a molecule. Therefore, these values given from the OZ plot of the in situ SAXS profile of molecules adsorbed in pores provide essential information on the cluster size and the adsorbed state of molecules in the pores.

GCMC simulation was carried out using the established procedures.[21−24] We used the 12-6 Lennard-Jones potential $\Phi_{ff}(r)$ for the fluid−fluid interaction at an intermolecular distance r using a single-center approximation.

$$\Phi_{ff}(r) = 4\epsilon_{ff}\left[\left(\frac{\sigma_{ff}}{r}\right)^{12} - \left(\frac{\sigma_{ff}}{r}\right)^{6}\right] \tag{4}$$

Here ϵ_{ff} and σ_{ff} are the CH_4−CH_4 potential well depth (ϵ_{ff}/k_B = 161.3 K) and the effective diameter (σ_{ff} = 0.3721 nm), respectively. Steele's 10-4-3 potential function was used for the interaction potential calculation of a N_2 molecule with a single graphite slab.[25]

$$\Phi_{sf}(z) = A\left[\frac{2}{5}\left(\frac{\sigma_{sf}}{z}\right)^{10} - \left(\frac{\sigma_{sf}}{z}\right)^{4} - \frac{{\sigma_{sf}}^4}{3\Delta_C(z + 0.61\Delta_C)^3}\right] \tag{5}$$

where A is $2\pi{\sigma_{sf}}^2\epsilon_{sf}\rho\Delta_C$, z is the vertical distance of the molecule from the graphite surface, ρ is the carbon atomic number density, and Δ_C is the interlayer distance of the graphite. ϵ_{sf} and σ_{sf} are fitted parameters of the CH_4−carbon potential depth and effective diameter, respectively, which were obtained using the Lorentz−Berthelot rules (ϵ_{sf} = 69.73 K, σ_{sf} = 0.3569 nm). The effective pore width w_{eff}, which is determined experimentally, is associated with the physical width H using eq 6.[26]

$$w_{eff} = H - (2z_0 - \sigma_{ff}) - \sigma_{ff}, \qquad z_0 = 0.856\sigma_{sf} \tag{6}$$

H is defined as the distance between opposite graphite surfaces, where z_0 is the distance of the closest approach between CH_4 and graphite surface.

The following established GCMC simulation method was applied to calculate the adsorption isotherm of CH_4. The random movement, creation, and removal of a molecule make a new configuration. They are accepted when they obey Metropolis's sampling scheme in proportion to $\exp(-\Delta E/(kT))$, where ΔE is the change of total energy in the system. We used a rectangular cell, $l \times l \times H$ (l = 6 nm), for the calculation of which size is replicated two-dimensionally to form an infinite slit-shaped pore.

3. Results and Discussion

The N_2 adsorption isotherms of P5 and P20 were of type I, indicating microporous solids of both ACFs. These isotherms were analyzed by the SPE method using the high-resolution α_S-plot. The micropore volume and average pore width, w_{eff}, were 0.25 mL g^{-1} for P5 and 0.91 mL g^{-1} for P20 and 0.7 nm for P5 and 1.1 nm for P20, respectively. The micropores of ACFs evaluated from N_2 adsorption at 77 K can be different from those from methane adsorption at 303 K. Hence, we determined the micropore structures of both ACFs for CH_4 by the comparison of experimental and simulated isotherms.

Figure 1a,b shows experimental and simulated adsorption isotherms of CH_4 at 303 K on P5 and P20. Here, the adsorbed amount is expressed by milligrams of adsorbed methane per milliliter of the micropore volume determined by N_2 adsorption at 77 K. P5 of narrower micropores has higher adsorbed density of CH_4 than P20 of wider micropores. As the density of liquid CH_4 is 440 mg ml^{-1} at boiling temperature (122 K), the maximum adsorbed density of methane in micropores of P5 at 303 K is about half of the density of bulk liquid methane at 122 K; methane molecules are highly packed in the micropores of P5 even at 303 K. We fitted experimental and simulated isotherms using the pore size distribution (PSD) of Gaussian function. The best fitting was obtained for the PSD shown in Figure 1c, leading to the w_{eff} = 0.6 nm for P5 and w_{eff} = 1.1 nm for P20. These values are similar to those determined by N_2 adsorption. A slight difference of the w_{eff} from N_2 and CH_4 adsorption in P5 should stem from the difference in their accessibility to micropores. While CH_4 molecules at 303 K can come into narrow micropores without any difficulty of diffusion, N_2 molecules cannot adsorb in narrower micropores due to the entrance blocking at 77 K. PSD of P5 is slightly broader than that of P20 in Figure 1c. Thus, both ACFs have considerably uniform micropores for CH_4, and both PSDs are different from

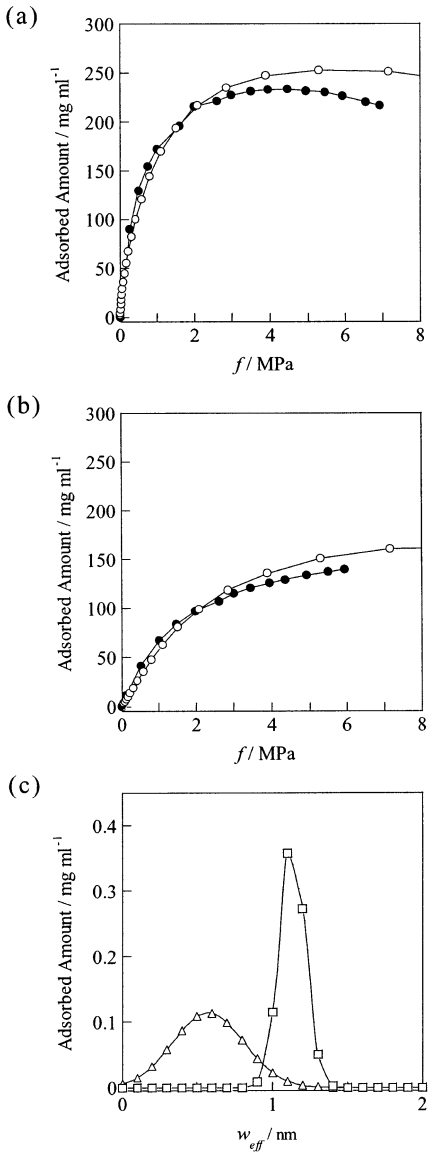

Figure 1. Adsorption isotherms of CH_4 on P5 (a) and P20 (b) and pore size distributions (c): for panels a and b, (●) experiment and (○) simulation; for panel c, P5 (△) and P20 (□).

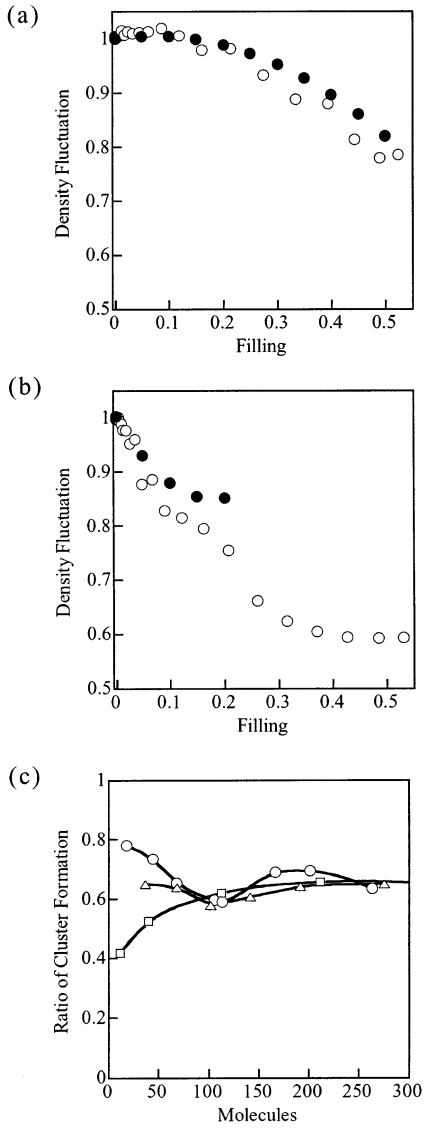

Figure 2. Density fluctuations of CH_4 on P5 (a) and P20 (b) and cluster formation ratios (c): for panels a and b, (●) experiment and (○) simulation; for panel c, (○) P5 (w_{eff} = 0.6 nm); (△) P20 (w_{eff} = 1.1 nm); (□) bulk state.

each other. Furthermore, experimental isotherms can be well described by the GCMC simulation. Accordingly, the detailed structural analysis of the snapshots from GCMC simulation for w_{eff} = 0.6 and 1.1 nm can be associated with the density fluctuation from in situ SAXS.

Figure 2a,b show the changes in the density fluctuations of adsorbed CH_4 on P5 and P20 with fractional filling ϕ, which is defined by the ratio of the volume occupied by adsorbed molecules to the micropore volume, from SAXS study and simulation. Here the experimental density fluctuation was obtained from the OZ-plot of in situ SAXS profile. The snapshot density function (SDF) from GCMC simulation can be calculated by summation of the site density fluctuation in each site volume (v) of 0.05^3 nm^3 over the whole simulation box.

$$\mathrm{SDF} = \sum_i (\Delta\rho_i)^2 v \tag{7}$$

Here $\Delta\rho_i$ is the electron density difference among CH_4, carbon, and pore space in the ith volume element of the simulation box. GCMC simulation also gives a good agreement with the experimental relation for both ACFs. Both density fluctuations from SAXS and GCMC simulation were normalized using each density fluctuation without CH_4 adsorption. The density fluctuation in P5 is almost constant until ϕ = 0.2 and gradually decreases above it. The density fluctuation change from SAXS is almost well described by the snapshot density fluctuation change for the w_{eff} = 0.6 system. This result suggests highly concentrated cluster formation of CH_4 below ϕ = 0.2. The density fluctuation gradually decreases with ϕ above ϕ = 0.2. On the other hand, the density fluctuation vs ϕ relation for P20 has no constant region at the initial adsorption near ϕ = 0. Hence, the cluster ratio of P20 is smaller than that of P5. The contribution of uniformly adsorbed CH_4 molecules in P20 should be larger than that in P5. As the adsorbed amount of CH_4 per unit pore volume of P20 is much smaller than that of P5, the density fluctuation vs ϕ relation for P20 from SAXS covers only a narrow ϕ region up to ϕ = 0.2. The SDF vs ϕ relation for w_{eff} = 1.1 nm can describe well the SAXS density fluctuation vs ϕ until ϕ = 0.1, showing a deviation above ϕ = 0.1. As the snapshots from GCMC simulation cannot clearly provide the quantitative information on the clusters, these snapshots were analyzed with so-called cluster analysis, which gives the size and number of clusters under GCMC simulation.[27,28] Figure 2c shows the cluster formation ratio from the cluster analysis. If all molecules are associated with the cluster formation, the cluster formation ratio is 1. Here, the abscissa is expressed by the molecules in the unit cell of the GCMC simulation. One hundred of the molecular number correspond to about ϕ = 0.28 for the w_{eff} = 0.6 nm system (P5) and to ϕ = 0.15 for the w_{eff} = 1.1 nm system (P20). The cluster formation ratio for the bulk gas in the volume at 303 K is also shown for comparison. One hundred of the molecules for the bulk gas correspond to that above 2 MPa. The cluster formation ratio of the w_{eff} = 0.6 nm system in the small molecular number is close to 0.8, decreasing to 0.6 at 100 of the molecular number. This is the greatest in three systems. This should stem from the presence of the remarkably enhanced interaction potential well; molecules should be adsorbed there to form clusters. Then, molecules occupy shallower potential sites to form fewer clusters around 100 of the molecular number. As the interaction potential profile of the wider pores (w_{eff} = 1.1 nm) have double minima of shallower depth than the minimum of the w_{eff} = 0.6 nm system, the cluster formation ratio is smaller than that of the w_{eff} = 0.6 nm system. Although highly compressed CH_4 gas has also a high cluster formation ratio, it is much smaller than those of CH_4 confined in these pores, if we compare them at the same CH_4 pressure. This clearly shows the marked compression effect of the nanorange molecular field of the micropores. Thus, the formation of highly concentrated clusters of CH_4 molecules in micropores can be explicitly shown regardless of application of relatively small pressures of 2−3 MPa. The ξ of eq 1 gives an approximated scale of the cluster size; the estimated average cluster sizes of CH_4 on P5 and P20 are 0.5 and 0.7 nm, respectively.

This clustering can be evidenced by the two-dimensional radial distribution function, as shown in Figure 3. Here, the two-dimensional radial distribution function, $\Psi(r)$, was calculated for the adsorbed layers parallel to the carbon wall.

$$\Psi(r) = \frac{N_r}{2\pi r\, \mathrm{d}r} \tag{8}$$

Here, N_r is the molecular number at distance r from a central molecule. Apparently, these two-dimensional radial distribution functions of CH_4 in pores have another peak (at 0.80 nm for the w_{eff} = 0.6 nm system and 0.85 nm for the w_{eff} = 1.1 nm

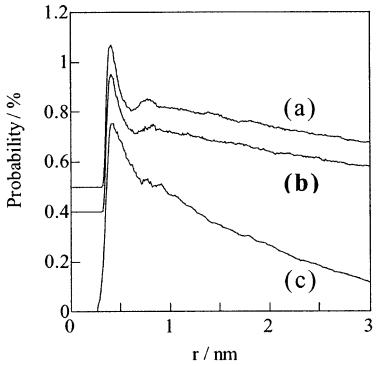

Figure 3. Two-dimensional radial distribution functions: (a) P5; (b) P20; (c) bulk.

system) in addition to the peak at 0.43 nm due to the nearest neighbor molecules. On the other hand, the bulk gas of 6 MPa has no such an additional peak. This second peak in the pore system indicates the presence of local structures extending the second neighbor distance in the case of CH_4 molecules adsorbed in pores. That is, the average two-dimensional diameter of the aggregated CH_4 should be in the range of 1.6−1.7 nm. Thus, a combination analysis of in situ high-pressure SAXS and GCMC simulation can elucidate the cluster structures of supercritical CH_4 confined in carbon micropores. This approach can be applied to another system.

Acknowledgment. This work was supported by Research Fellowship of the Japan Society for the Promotion of Science for Young Scientists and by Grant-in-Aid for Fundamental Scientific Research S.

References and Notes

(1) Alcañiz-Monge, J.; Casa-Lillo, M. A.; Cazorla-Amorós, D.; Linares-Solano, A. *Carbon* **1997**, *35*, 291.

(2) Zhou, L.; Zhou, Y.; Li, M.; Chen, P.; Wang, Y. *Langmuir* **2000**, *16*, 5955.

(3) Lozano-Castelló, D.; Cazorla-Amorós, D.; Linares-Solano, A.; Quinn, D. F. *Carbon* **2002**, *40*, 989.

(4) Zhang, X.; Wang, W. *Fluid Phase Equilibria* **2002**, *194*−*197*, 289.

(5) Chen, X. S.; McEnaney, B.; Mays, T. J.; Alcañiz-Monge, J.; Cazorla-Amoros, D.; Linares-Solano, A. *Carbon* **1997**, *35*, 1251.

(6) Murata, K.; Kaneko, K. *Chem. Phys. Lett.* **2000**, *321*, 342.

(7) Tanaka, H.; El-Merraoui, M.; Steele, W. A.; Kaneko, K. *Chem. Phys. Lett.* **2002**, *352*, 334.

(8) Iiyama, T.; Nishikawa, K.; Otowa, T.; Kaneko, K. *J. Phys. Chem.* **1995**, *99*, 10075.

(9) Iiyama, T.; Ruike, M.; Kaneko, K. *Chem. Phys. Lett.* **2000**, *331*, 359.

(10) Ohkubo, T.; Yang, C.-M.; Raymundo-Pinero, E.; Linares-Solano, A.; Kaneko, K. *Chem. Phys. Lett.* **2000**, *329*, 71.

(11) Ohkubo, T.; Iiyama, T.; Nishikawa, K.; Suzuki, T.; Kaneko, K. *J. Phys. Chem. B* **1999**, *103*, 1859.

(12) Ohkubo, T.; Iiyama, T.; Kaneko, K. *Chem. Phys. Lett.* **1999**, *312*, 19.

(13) Miyawaki, J.; Kaneko, K. *Chem. Phys. Lett.* **2001**, *337*, 243.

(14) Kaneko, K.; Murata, K. *Adsorption* **1997**, *3*, 197.

(15) Menon, V. C.; Komarneni, S. *J. Porous Mater.* **1998**, *5*, 43.

(16) Suzuki, T.; Kaneko, K.; Gubbins, K. E. *Langmuir* **1997**, *13*, 2545.

(17) Radhkrishnan, R.; Gubbins, K. E.; Watanabe, A.; Kaneko, K. *J. Chem. Phys.* **1999**, *111* (19), 9058.

(18) Ohba, T.; Kaneko, K. *J. Phys. Chem. B* **2002**, *106*, 7171.

(19) Ornstein, L. S.; Zernike, F. *Proc. R. Akad., Amsterdam* **1914**, *17*, 793.

(20) Nishikawa, K.; Tanaka, I. *Chem. Phys. Lett.* **1995**, *244*, 149.

(21) Cracknell, R. F.; Nicholson, D.; Quirke, N. *Mol. Phys.* **1993**, *80* (4), 885.

(22) Maddox, M.; Ulberg, D.; Gubbins, K. E. *Fluid Phase Equilibria* **1995**, *104*, 145.

(23) Bojan, M. J.; Steele, W. A. *Carbon* **1998**, *36*, 1417.

(24) Ohba, T.; Kaneko, K. *Langmuir* **2001**, *17*, 3666.

(25) Steele, W. A. *Surf. Sci.* **1973**, *36*, 317.

(26) Kaneko, K.; Cracknell, R.; Roger, F.; Nicholson, D. *Langmuir* **1994**, *10*, 4606.

(27) Coverdale, G. N.; Chantrell, R. W.; Martin, G. A. R.; Bradbury, A.; Hart, A.; Parker, D. A. *J. Magn. Magn. Mater.* **1998**, *188* (1−2), 41.

(28) Aoshima, M.; Suzuki, T.; Kaneko, K. *Chem. Phys. Lett.* **1999**, *310*, 1.